Copyright

by

Uyen Nguyen Phuong Huynh

2011

The Thesis Committee for Uyen Nguyen Phuong Huynh
Certifies that this is the approved version of the following thesis :

Hybrid Photovolvoltaic Devices Based on Nanocrystals and Conducting Metallopolymers Using the Seeded Growth Method

APPROVED BY
SUPERVISING COMMITTEE:

Supervisor:

Bradley J. Holliday

Richard A. Jones

Hybrid Photovolvoltaic Devices Based on Nanocrystals and Conducting Metallopolymers Using the Seeded Growth Method

by

Uyen Nguyen Phuong Huynh, BS

Thesis

Presented to the Faculty of the Graduate School of

The University of Texas at Austin

in Partial Fulfillment

of the Requirements

for the Degree of

Master of Arts

The University of Texas at Austin

August 2011

Dedication

To my parents, my grandma and my uncle for giving me life, peace, love, strength, and passion in chemistry. To my family and friends for supporting and guiding me through the toughest times in my life.

Acknowledgements

I ‘d like to thank Dr. Bradley J. Holliday for being a wonderful mentor and helping me to build stronger research experience and self-confidence. Thank you for being understanding and supporting to guide me through the toughest times in the last two years. In addition, I would like to thank Dr. Richard A. Jones for being my committee member, supporting and providing suggestion to my research projects.

I’d like to thank everyone in Holliday group for the great friendship and generous help and support.

Aug 1, 2011

Abstract

Hybrid Photovolvoltaic Devices Based on Nanocrystals and Conducting Metallopolymers Using the Seeded Growth Method

Uyen Nguyen Phuong Huynh, M.A.

The University of Texas at Austin, 2011

Supervisor: Bradley J. Holliday

Described herein are two projects focusing on developing and investigating two types of nanoparticles (NPs) grown by the seeded growth method from a conducting metallopolymer for photovoltaic (PV) applications. Core/shell CdS/ZnS NPs are proven to resist the photo-oxidation of PV devices, while $CuIn_xGa_{(1-x)}Se_2$ (CIGS) NPs are expected to optimize the efficiency of PV devices.

Table of Contents

List of Tables ix

List of Figures x

List of Schemes xii

Chapter 1 1

Introduction 1

1.1 Conjugated polymer and photovoltaic application 1

1.2 Photovoltaic devices 2

1.2.1 Principles of operation and types of PV cells 2

1.2.2 Bulk heterojunction PV cells 4

1.3 Inorganic NP and photovoltaic application 6

1.3.1 Nanoparticle-polymer PV cells operation principles 6

1.3.2 Inorganic nanoparticle 8

1.3.3 Challenges in colloidal synthesis in PV cells and seeded growth method 9

Chapter 2 13

Photo-oxidation Resistance Effect of Core/shell CdS/ZnS Nanoparticles Grown by Seeded Growth from a Conducting Metallopolymer Matrix 13

2.1 Introduction 13

2.2 Experimental 15

2.2.1 Synthesis of cadmium salen complex (A) 16

2.2.2 Electropolymerization 16

2.2.3. Seeded Growth Procedure for CdS/ZnS Nanoparticles 17

2.2.4. Photo-oxidation experiment 19

2.2.5 Transmission Electron Microscope 19

2.3 Results and discussion 20

2.3.1 TEM images and analysis of NPs size and d-spacing 20

2.3.2 EDX analysis 22
2.3.3 Photo-oxidation analysis 23
2.3.4 XPS analysis 27
2.4 Conclusion 29

Chapter 3 30

Direct Synthesis of CIGS Nanoparticles within Conducting Metallopolymer Matrix for Hybrid Photovoltaic 30
3.1 Introduction 30
3.2 Experimental 32
3.2.1 Synthesis of copper salen complex (A) 32
3.2.2. Electropolymerization 32
3.2.3 Seeded Growth Procedure for CIGS Nanoparticles 33
3.2.4 Transmission Electron Microscope 33
3.3 Results and discussion 34
3.3.1 TEM images and analysis of NPs size and d-spacing 34
3.3.2 EDS analysis 36
3.4 Conclusions 38

List of Tables

Table 1. Summary of EDX composition for thin film composed of **Pol** and CdS or CdS/ZnS of various compositions grown on **Pol**.....23

Table 2. Summary of EDX composition for thin film composed of CIGS(2X) or CIGS(4X) NPs grown on **Pol** 36

List of Figures

Figure 1. Four device architectures of conjugated polymer-based photovoltaic cells 3

Figure 2. Diagram depicting portion of (a) heterojunction bilayer and (b) bulk heterojunction. 5

Figure 3. Energy levels and the harvesting of energy from a photon for the PV cell depicted in the inset.[9] 7

Figure 4. Radiation spectrum and intensity of fluorescent light bulb.....19

Figure 5. TEM images of photovoltaic thin films with different compositions: Pol (A), CdS(2X) (B), and CdS(2X)/ZnS(2X) (C) 21

Figure 6. HRTEM images of hybrid thin films with CdS NPs (left) and CdS/ZnS NPs (right) 22

Figure 7. UV-Vis absorption spectra of thin films of various compositions exposed to atmosphere and visible light in 0 hour (top) and 835 hours (bottom).25

Figure 8. Degradation percentage of the optical absorption at 500 nm of thin films with various compositions 26

Figure 9. XPS core-level spectra of sulfur S 2p at different stages of degradation of thin films composed of **Pol** and CdS(2X) NPs (top), **Pol** and CdS(2X)/ZnS(2X) NPs (middle), and **Pol** and CdS(2X)/ZnS(4X) NPs (bottom).....28

Figure 10. Low cost, non-vacuum methods for CIGS deposition.[54].....31

Figure 11. TEM images of thin film made of different compositions: Pol (A), Pol and CIGS (2X) (B), and Pol and CIGS (4X) (C).....35

Figure 12. EDX spectra of thin film made of **Pol**.....37

Figure 13. EDX spectra of thin film composed of **Pol** and CIGS (2X) NPs 37

Figure 14. EDX spectra of thin film composed of **Pol** and CIGS (4X) NPs 38

List of Schemes

Scheme 1. Seeded growth approach to the preparation of hybrid electronic material 12

Scheme 2. Seeded growth procedure for CdS/ZnS NPs 18

Chapter 1

Introduction

Hybrid photovoltaic (PV) devices utilize a photoactive layer which is a composite of organic and inorganic semiconductors. This thesis focuses on bulk heterojunction (BHJ) devices composed of an organic conducting polymer and inorganic nanoparticles (NPs).

1.1 Conjugated polymer and photovoltaic application

Π-Conjugated polymers are organic semiconductors having π–electron density delocalized along the polymer chain.[1] Conjugated polymers became attractive for photovoltaic applications due to their low cost, property of easily being cast into flexible thin film in large scale, and high optical absorption coefficient. Conjugated polymers such as poly(3-hexylthiophene) (P3HT), poly[2-methoxy-5-(2'-ethylhexoxy)-1,4-phenylenevinylene] (OC_1C_{10}-PPV), poly[2-methoxy, 5-(2-ethylhexoxy)-1,4-phenylene vinylene] (MEH-PPV), which are soluble in common organic solvents, are good candidates for wet-processing techniques such as spin casting, dipcoating,[2] ink jet printing,[3,4] screen printing,[5-7] and micromolding.[6] Conjugated polymers are capable of absorbing a significant amount of the photons from sunlight due to high peak optical absorption coefficients. PV cells made of conjugated polymers of direct band gap can be 100-500 nm in thickness; while crystalline silicon PV cells need to be approximately 100

μm thick for efficient absorption of sunlight. However, only a fraction of the solar spectrum can be converted into electricity with organic semiconductors, this is due to the mismatch between the peak of photon flux of the AM1.5G solar spectrum (around 700 nm, 1.8 eV) and the absorption peak of P3HT, MEH-PPV, and OC_1C_{10}-PPV (350-650 nm, 3.5-1.9eV). [8]

1.2 Photovoltaic devices

1.2.1 Principles of operation and types of PV cells

There are five consecutive steps in the process of charge separation and transportation within organic PV cells, i.e., (1) photon absorption, (2) exciton diffusion, (3) exciton dissociation, (4) charge carrier transport, and (5) charge collection at electrodes.[9] In a PV cell in which a polymer acts as the photon absorber, when the absorbed photon energy is greater than polymer's band gap (E_g) , polymer electrons are promoted from the HOMO to the LUMO to form neutral excitons which are considered as coulombically bound electron-hole pairs.[9] Excitons then diffuse through the polymer matrix and dissociate into charge carriers at the semiconductor interface, i.e., holes and electrons. Charge carriers transport through the film by a hopping process, and are then collected at the electrodes.

Figure 1 illustrates the four device architectures of conjugated polymer-based PV cells; 1(a) is the structure of single layer PV cells while the other three are semiconductor

junction PV cells. Disordered bulk heterojuntion PV cells, like those shown in 1(c), are employed in the projects discussed in this thesis.

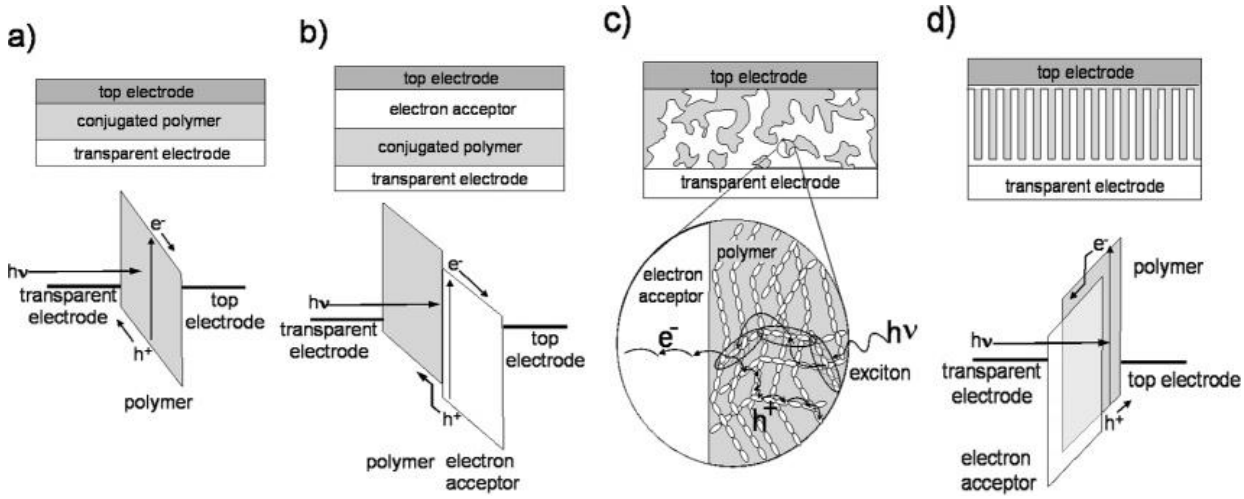

Figure 1. Four device architectures of conjugated polymer-based photovoltaic cells (a) single-layer PV cell; (b) bilayer PV cell;(c) disordered bulk heterojunction; (d) ordered bulk heterojunction.[8]

PV cells made of a single layer of conjugated polymer display very low power conversion efficiencies (PCE) which is typically below 0.1%[10] while commercial crystalline silicon can advance up to 15%.[11] In conjugated polymers, photogenerated electrons and holes are strongly coupled and tend to recombine and result in the low conversion efficiency. Recombination phenomena occur due to the nature of bound excitons, and the mobilities of charge carriers in conjugated polymers. At room temperature, generated bound excitons in these materials tend to decay rather than dissociate.[12] In addition, the low mobilities of the charge carriers raise the possibility for hole and electron recombination.[8] It is reported that hole mobilities for conjugated

polymers range from 10^{-1} to 10^{-7} $cm^2/(V\ s)$[13-16] and electron mobilities range from 10^{-4} to 10^{-9} $cm^2/(V\ s)$[14,17] while hole and electron mobilities in crystalline silicon are significantly higher, up to 475-1500 $cm^2/(V\ s)$.[18]

Hybrid PV cells are addressed to solve the recombination problem with an interface between two semiconductor components which serve as electron donor and electron acceptor. When there is an energy difference (offset) between the LUMO of electron donor and acceptor, excitons are provided energy to dissociate instead of decay, and generated holes and electrons diffuse into hole acceptor (electron donor) and electron acceptor (hole donor) pathways. Bilayer PV cells and disordered bulk heterojunction cells will be discussed further in section 1.2.2. Ordered bulk heterjunctions are is the ideal PV device architecture, shown schematically in Figure 1d. In this structure, each semiconductor has continuous domains and is connected to only one electrode; the interface between them is maximized while the diffusion domains for excitons and charge carriers are minimized. This structure is expected to improve the transportation of charge carriers to the electrodes and to avoid them getting trapped on isolated acceptors with domain sizes larger than the exciton diffusion length.[8]

1.2.2 Bulk heterojunction PV cells

A hybrid PV cell is made of two different semiconductor components. The interface between them allows photogenerated holes and electrons to dissociate and travel in opposite directions until they reach the photoanode and photocathode respectively.

Recombination phenomenon is dominant in a single layer of conjugated polymer based PV cells while exciton dissociation is favorable in hybrid PV cells.

In single layer and bilayer photovoltaic cells, photogenerated excitons cannot reach the electrode or the interface as the absorption length of conjugated polymers is around 100 nm while the exciton diffusion length (L_{ex}) in several conjugated polymer is only 4-20 nm.[19-23] In bilayer PV cells, the average polymer phase domain size (L_{pol}) is larger than L_{ex}, thus a large fraction of the photogenerated excitons cannot reach the interface to dissociate. Disordered bulk heterojunctions shows higher PCE as the distance excitons must travel to reach the interface is shortened, and the interface area is greater.[9] See Figure 2.

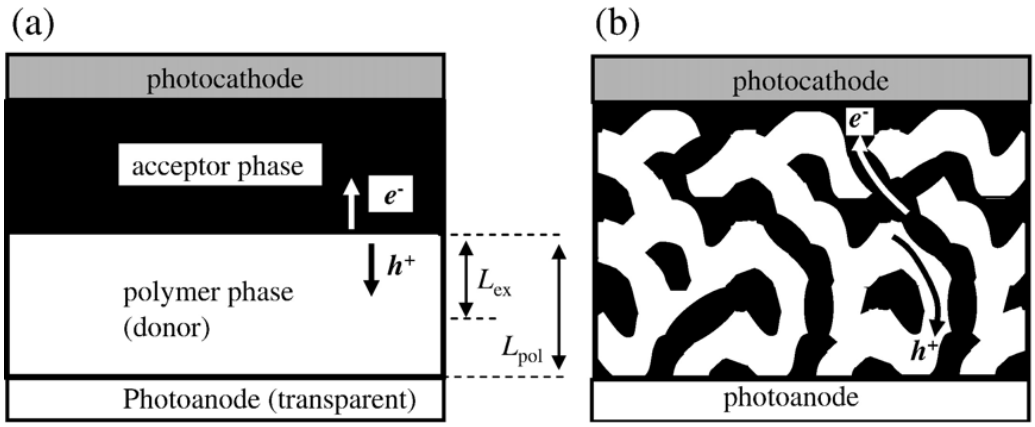

Figure 2. Diagram depicting portion of (a) heterojunction bilayer and (b) bulk heterojunction.
The latter is assumed to consist of a bicontinuous donor and acceptor phase. The diagram for (a) is not drawn to scale. Most of the polymer phase is further from the interface than L_{ex}. However, in (b) a much higher proportion of the polymer phase is less than a distance of L_{ex} from the interface. In that case L_{pol} represents the mean domain size of the polymer phase.[9]

1.3 Inorganic NP and photovoltaic application

1.3.1 Nanoparticle-polymer PV cells operation principles

One type of bulk heterojunction PV cell is a PV cell composed of conjugated polymers and inorganic NP which are able to absorb visible light. In these devices, photogenerated excitons from the LUMO of the polymer diffuse to polymer/NP interface and dissociate into holes and electrons. The electron is then accepted into the LUMO of the inorganic NP which have relatively low electron affinity.[9,24,25] Hole and electron transport toward the photocathode and photoanode, respectively, promote the generation of photocurrent and reduce the possibility of charge recombination. Figure 3 describes schematically the structure of a hybrid NP-polymer bulk heterojunction PV cell and charge separation and transport within it. A photoactive layer composed of P3HT polymer and NP, e.g. ZnO, CdSe, etc. is sandwiched between ITO, PEDOT:PSS and an Al electrode.

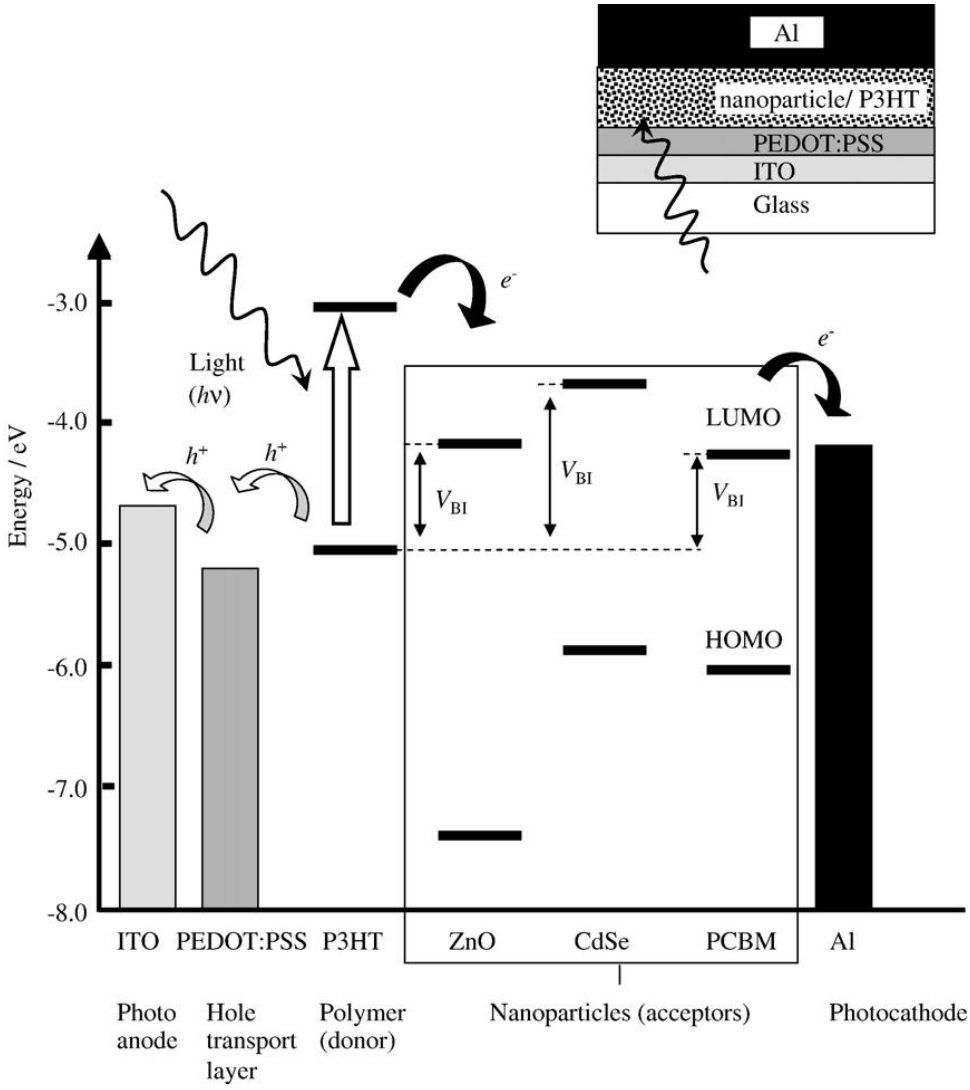

Figure 3. Energy levels and the harvesting of energy from a photon for the PV cell depicted in the inset.[9]
The photoactive layers considered here would contain P3HT and either ZnO, CdSe, or PCBM acceptors. Open circuit conditions are taken to apply. Built-in voltage (V_{BI}) for PV cells results from the energy difference of the HOMO of the polymer donor and the LUMO of NP acceptor.

1.3.2 Inorganic nanoparticle

The performance of PV cells varies with different combinations of conducting polymer and NP; promising polymers include OC_1C_{10}-PPV, P3HT, poly(2,7-(9,9-dioctyl-fluorene)-alt-5,5-(4',7' -di-2-thienyl-2',1',3'-benzothiadiazole)) (APFO-3), Poly(2-methoxy-5-(3'-7'-dimethyloctyloxy)-1,4-phenylenevinylene) (MDMO-PPV), MEH-PPV, and NP in conjunction with them are CdSe, ZnO, PbS, PbSe, TiO_2, TiO_2-HgTe, $CuInSe_2$.[9] In 2008, the combination of P3HT/CdSe established the highest PCE value of 2.8% for hybrid devices.[26]

NP-polymer photoactive layers are made by blending NPs with polymer,[9] thus, inorganic NPs, e.g. CdSe, are commonly chelated with organic surfactant, e.g. TOPO (trioctylphosphine oxide), to increase their dispersability in polymer solution. It is observed that the efficiency of PV devices depends on the geometry, the aspect ratio,[27] the weight fraction[25] and the size[2] of the NPs, and the side chain structure of the polymer.[24]

NPs used in PV devices can be nanocrystals, nanorods, tetrapods, or hyperbranched architectures. Hyperbranched NPs are argued to bring out the most efficient charge transfer pathway for maximum PCE at lower volume fraction than other NP geometries.[28] NPs with higher aspect ratios are observed to improve PCE as electron transport is favored by conduction band movement rather than hopping mechanisms which occurs in shorter NPs.[27] Weight fraction of NPs also plays an important role in photovoltaic efficiency, as the increase in the NP weight fraction allows formation of a

good percolation path through NP and polymer, and consequently improves electron transport.[25]

The size of NPs was proposed to affect PV cell efficiency, and the effect appears to vary with different hybrid PV cell components. Ginger and Greenham found NP diameters ranging from 2.5 to 4.0 nm shows no effect on efficiency of MEH-PPV/CdSe device. However, it is expected that smaller NPs possesses lower electron affinity due to the quantum confinement effect but this work shows that the smallest NPs have sufficient electron affinity to allow electron transfer from MEH-PPV.[24] Hybrid PV cells composed of P3HT and Si nanocrystals show that open-circuit voltage (V_{oc}) and short circuit current (I_{sc}) are inversely related to NP size. PCE is highest for devices made from P3HT and Si NPs with diameters of 3-5 nm, decreases with 5-9 nm NPs, and is lowest with 9-10 nm NPs.[29] On the other hand, de Freitas et al. proved that increasing CdSe NP size from 2.0 to 4.0 nm enhances the short-circuit current (I_{sc}) of the PFT/CdSe/PCBM devices. Larger NP are proposed to contribute to the formation of more excitons or a more accessible percolation network.[30]

1.3.3 Challenges in colloidal synthesis in PV cells and seeded growth method

The development of low-cost and high-efficiency NP-polymer cells encounters problems associated with NP-polymer interactions and morphology control. Poor NP-polymer interaction incites charge recombination and limits the efficiency of charge separation and transport in NP-polymer devices.[9,30] One of the morphological effects

could enhance PCE of NP-polymer PV cells is controlling NP aggregation to form accessible percolation network, thus improving charge separation and transport.[30,31]

Polymers in solution have a tendency to bind to NPs, or to remain coiled and non-adsorbed depending on the strength of the interaction with NPs. Adsorption is favored when the interaction between NPs and polymer chains is strong, and strongly adsorbed polymer chains have fewer tails and loops, which are the ends and portions of polymer chain remained unabsorbed to the NPs. A weak NP/polymer interaction results in a greater proportion of polymer tails and loops, and in the extreme case of weak interaction leads to non-absorbed polymer. In addition, the adsorption of polymer decreases when NP size is reduced, e.g. weak interaction between PCBM NP of 1 nm diameter in P3HT results in PCBM diffusion during annealing, thus, limitations in device efficiency.[32,33]

NP aggregation is one factor that lowers device performance. The physical forces driving NP aggregation is poor NP/polymer interactions, non-adsorbed polymer, and interparticle interaction during solvent evaporation.[9,27,28,34] Morphology of the photoactive layer is governed by the stability of the NP-polymer-solvent dispersion which depends heavily on the extent of adsorption between NP and polymer. Blending of NPs with non-adsorbed polymer leads to depletion flocculation, which happens when polymer size is larger than NP, thus, polymer coils are excluded from the space between the NPs and the osmotic pressure induces flocculation of NP.[35] Flocculation is incited with increasing cross-sectional area of the deletion zone between NP, thus, aggregation

occurs easily for high aspect-ratio NPs. Attraction between neighboring NPs increases when NP-rich regions are parallel to each other and the NP volume fraction is high.[36]

With many issues relating to dispersion stability of blended mixtures in the NP-polymer fabrication procedure, researchers have started to shift their attention to the direct synthesis of NP within the polymer matrix. Several groups employed the method of mixing NP precursors into polymer-containing solution,[37-39] while others, e.g. Mejía et al., have grown NPs from the metal seed points embedded in a metallopolymer thin film by treating the thin film with a NP precursor solution.[40]

Luccio et al. grew CdS NP by the thermolysis of dispersed cadmium thiolate precursor molecules (powder) in polystyrene and Cyclic Olefin Copolymer (COC) solution,[38] also Radchenko et al. induce formation of $CdCl_2$ NP in a polyethylene oil solution melt through which hydrogen sulfide is then bubbled and the result is the formation of CdS.[39]

Mejía et al. in our group has developed a hybrid photovoltaic material based on the seeded growth of CdS NPs within a conducting metallopolymer matrix.[41] This method was utilized to provide direct physical and electronic contact between these two photoactive components in order to eliminate problems associated with colloidal synthesis, i.e. surfactant/capping agents, and aggregation of NP. Seeded growth is a simple and low-cost process at room temperature to grow NP from metal seed points embedded directly in the conducting polymer backbone. The CdS seeded growth procedure is depicted in Scheme 1. An inorganic cadmium complex, which contains

polymerizable bithiophene end groups attached to a salen-type ligand which is the binding site for cadmium [39] ions, was synthesized and then electropolymerized to form a conducting metallopolymer. Thin films are treated with sequential cycles of soaking in a solution of Cd (II) salt and then dissolved hydrogen sulfide, CdS NP are nucleated from the Cd seed points on the metallopolymer backbone.[40]

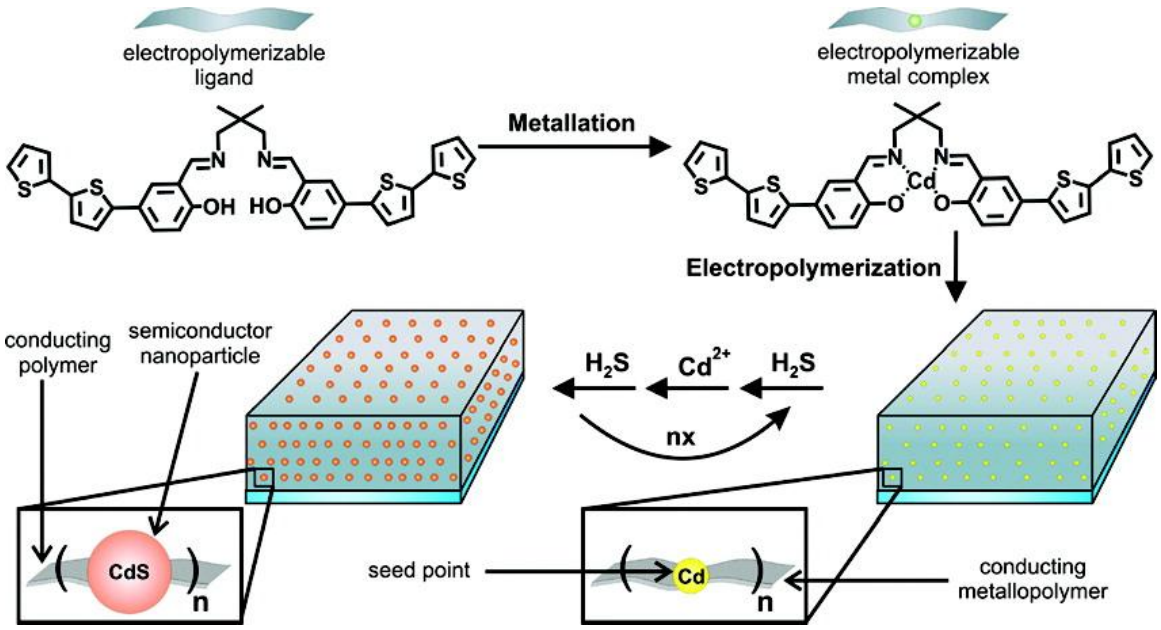

Scheme 1. Seeded growth approach to the preparation of hybrid electronic material.[40]

Chapter 2

Photo-oxidation Resistance Effect of Core/shell CdS/ZnS Nanoparticles Grown by Seeded Growth from a Conducting Metallopolymer Matrix

2.1 Introduction

Over the last few decades, research in the field of the organic photovoltaic (OPV) devices has been growing tremendously. The major trend in OPV research is to improve the power conversion efficiency (PCE) of the OPV device as much as possible. However, there has been relatively little attention given to the stability of these devices. There have been a number of studies revealing that most polymer solar cells decay in a matter of hours or within a few months, while the inorganic silicon-based solar cells last up to 25 years. Unfortunately, the contributing factors and mechanism of degradation are complicated and not yet fully understood. In OPV devices the degradation targets all device components, ITO electrode, PEDOT:PSS layer, photoactive layer, and metal electrode through chemical, physical and mechanical degradation processes.[42]

The project herein focuses on the photo-oxidation process of a nanoparticle-polymer photovoltaic (PV) film, in which the nanoparticle (NP) is CdS and the monomer is composed of polymerizable bithiophene end groups and salen-type ligand. Our group has developed a hybrid PV material based on the seeded growth of CdS NPs within a

conducting metallopolymer matrix.[40] This method was utilized to provide direct physical and electronic contact between these two photoactive components in order to eliminate problems associated with colloidal synthesis, such as surfactant/capping agents and aggregation of NPs. Seeded growth is a simple and low-cost process conducted at room temperature which grows NPs from metal ion seed points embedded directly in the conducting polymer backbone.[40]

The degradation of the NP-polymer film is not fully understood as there have been very few studies about the photo-oxidation of hybrid PV cells. Under UV illumination and presence of oxygen, TiO_2, which is the photoactive material most commonly employed in hybrid PV cells, generates electron-hole pairs. The photogenerated electrons are transferred to bound oxygen (O_2) and form the superoxide radical anion $O_2^{\bullet -}$. Meanwhile, the photogenerated holes react with surface hydroxyl group to form $TiOH^{\bullet +}$. Both of these radical species can oxidize organic compounds including polymers.[42] Hintz et al. proposed photo-oxidation mechanism for poly(3-hexylthiophene) (P3HT) which includes the primary attack of oxygen at the alkyl chain and at the terminal thiophene rings in radical chain reactions.[43]

NPs are also susceptible to photo-oxidation as surface atoms are not fully coordinated and highly reactive. In CdS NPs, photo-oxidation occurs when surface sulfide atoms become oxidized in the presence of oxygen and a hole.[44] On the other hand, surface cadmium atoms can trap delocalized excited electrons, and this leads to the poor electronic accessibility.[45] Core/shell structured CdS/ZnS was reported to solve the above

problem thanks to the hole-confinement effect explained by molecular orbital theory. CdS (core) and ZnS (shell) composites have LUMO energy levels relatively close to each other, thus mixing strongly and a new LUMO will be delocalized throughout the structure. This mixing is the reason why electrons delocalize throughout the entire NP. However, the HOMO energy level of the shell is much lower than the core, thus the HOMO of the core/shell nanostructure has corelike character, and the holes are confined mostly to the core. [45] In these structures, photo-oxidation is expected to be delayed when the holes are confined to the core and the cadmium atoms are passivated with the ZnS shell.

2.2 Experimental

The hybrid photovoltaic material investigated herein is a composite made from a conducting metallopolymer and CdS/ZnS NPs. The metallopolymer thin film was deposited onto an ITO coated glass substrate using electropolymerization, and is a copolymer **Pol** composed of monomer **A** shown in Figure 1 and bithiophene (BT) in 1:50 ratio. CdS NPs nucleate from cadmium [39] ions bond to the salen moiety of monomer A.

The following chemicals were used as received: cadmium nitrate tetrahydrate (Alfa Aesar), zinc acetate dehydrate (Strem Chemicals), hydrogen sulfide gas (Matheson Tri-Gas). All solvents were dried using an Innovative Technology, Pure Solv solvent purifier . All reactions were performed with standard Schlenck techniques. Absorption spectra were recorded on a Varian Cary 6000i UV-VIS-NIR spectrophotometer with

Starna Quartz fluorometer cells with a pathlength of 10 mm. Nanoparticle characterization was performed with Transmission Electron Microscope (TEM). Chemical composition of thin film's surface were analyzed by X-ray photoelectron spectroscopy (XPS) carried out on a PHI 5700 XPS system equipped with dual Mg X-ray source and monochromatic Al X-ray source complete with depth profile and angle-resolved capabilities.

2.2.1 Synthesis of cadmium salen complex (A)

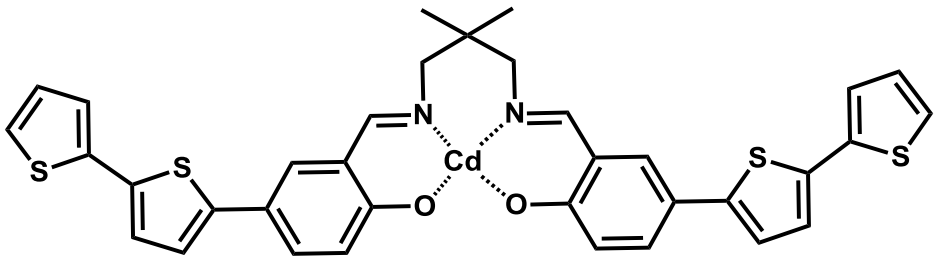

Synthesis of cadmium salen complex (A) was described previously in the literature.[40]

2.2.2 Electropolymerization

Metallopolymer thin film **Pol** was electropolymerized from a $2x10^{-4}$ M CH_2Cl_2 solution of **(A)** with bithiophene in a ratio of 1:50 by cycling between -0.5V and 1.5V at ν=100 mVs^{-1} for 5 scans under nitrogen atmosphere in a glovebox using GPES system from Eco. Chemie B. V.. The electrolyte used was 0.1 M tetrabutylammonium

hexaflourophosphate [(*n*-Bu)$_4$N][PF_6] TABPF6. Electrochemical experiments were performed in a three-electrode cell with a Ag/$AgNO_3$ non-aqueous reference electrode, a working electrode, and a Pt wire coil counter electrode.[40] Different working electrodes were used for characterization with different instruments, i.e. UV-Vis Absorbance Spectroscopy, TEM, and XPS. A sample for UV-Vis absorbance spectroscopy characterization were prepared by electropolymerizing a thin film onto an Indium Tin Oxide (ITO) coated glass purchased from Delta Technologies, Limited. A sample for TEM characterization were prepared by electropolymerizing a thin film onto a carbon coated gold TEM grids purchased from Electron Microscopy Sciences. A sample for XPS characterization were prepared by electropolymerizing a thin film onto stainless steel purchased from Small Parts, Inc.

2.2.3. Seeded Growth Procedure for CdS/ZnS Nanoparticles

The electropolymerized thin films went through a series of core/shell growing cycles, and each cycle consist of one core CdS growth cycle followed by one shell ZnS growth cycle.

A CdS growth cycle consists of the three following steps. The electropolymerized thin films were exposed to gaseous hydrogen sulfide (H_2S) for three minutes, and then rinsed thoroughly with dry CH_2Cl_2. The films were then soaked in a solution of $Cd(NO_3)_2$ in CH_2Cl_2/MeOH (2.03×10^{-3} M) for one minute followed by rinsing with dry CH_2Cl_2.

Last, the films were were exposed to gaseous hydrogen sulfide (H_2S) for three minutes, and then rinsed thoroughly with dry CH_2Cl_2.

A ZnS growth cycle consists of the three following steps. The electropolymerized thin films were exposed to gaseous hydrogen sulfide (H_2S) for three minutes, and then rinsed thoroughly with dry CH_2Cl_2. The films were then soaked in a solution of $Zn(CH_3COO)_2$ in CH_2Cl_2/MeOH (2.03×10^{-3} M) for one minute followed by rinsing with dry CH_2Cl_2. Last, the films were were exposed to gaseous hydrogen sulfide (H_2S) for three minutes, and then rinsed thoroughly with dry CH_2Cl_2.

The thin film which went through 1 cycle (1X) of core and shell growth is named CdS(1X)/ZnS(1X). See Scheme 2.

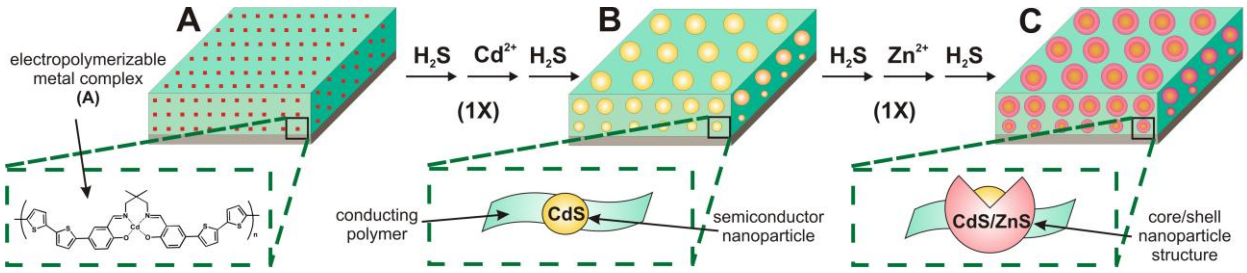

Scheme 2. Seeded growth procedure for CdS/ZnS NPs.

2.2.4. Photo-oxidation experiment

Photo-oxidation experiment is performed by exposing photovoltaic thin films to the radiation emitted from high output 200 watt compact fluorescent spectrum bulb, see Figure 4. The thin films were exposed continuously to the above visible light source. UV-Vis and XPS spectra were collected when the thin films were freshly prepared and then collected in sequence of several hundred hours along the photo-oxidation process.

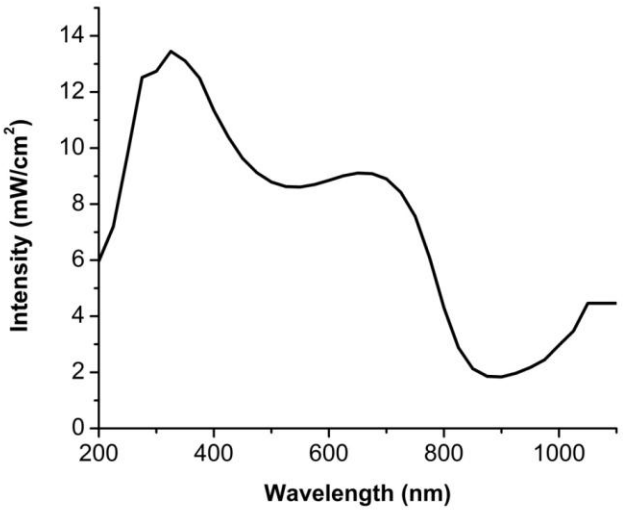

Figure 4. Radiation spectrum and intensity of fluorescent light bulb.

2.2.5 Transmission Electron Microscope

TEM experiments were performed using JEOL 2010F microscope configured with Oxford INCA energy dispersive spectrometer. Nanoparticle analysis was done using Gatan Digital Micrograph software. A sample for TEM characterization was

prepared by electropolymerizing a thin film of Pol onto a carbon coated gold TEM grids purchased from Electron Microscopy Sciences. The films were kept in air free environment and nanoparticles were grown with seeded growth method described above.

2.3 Results and discussion

2.3.1 TEM images and analysis of NPs size and d-spacing

Transmission Electron Microscope (TEM) was employed to investigate NP size, d-spacing, and elemental composition. See figure 5. Thin film A is composed of **Pol** only and no NPs was depicted in this figure. Thin film B contains CdS(2X) NPs with an oval shape and the average size for the CdS core is 6.8 nm in length and 4.2 nm in width. After 2 cycles of shell growth, the thin film C has CdS(2X)/ZnS(2X). The NP average size extends to 9.1 nm x 7 nm. There is no significant change in d-spacing of the NPs before and after the growth of the shell, the observed d-spacing values range from 0.3 nm to 0.39 nm, while reported d-spacing of CdS is 0.33 nm[46] and of ZnS is 0.31 nm.[47] See figure 6. Epitaxial growth is expected as the CdS and ZnS d-spacing are similar to each other, this matching can lead to the uniform passivation of the NP surface and possibility of minor reconstruction of the surface at the atomic level.[48]

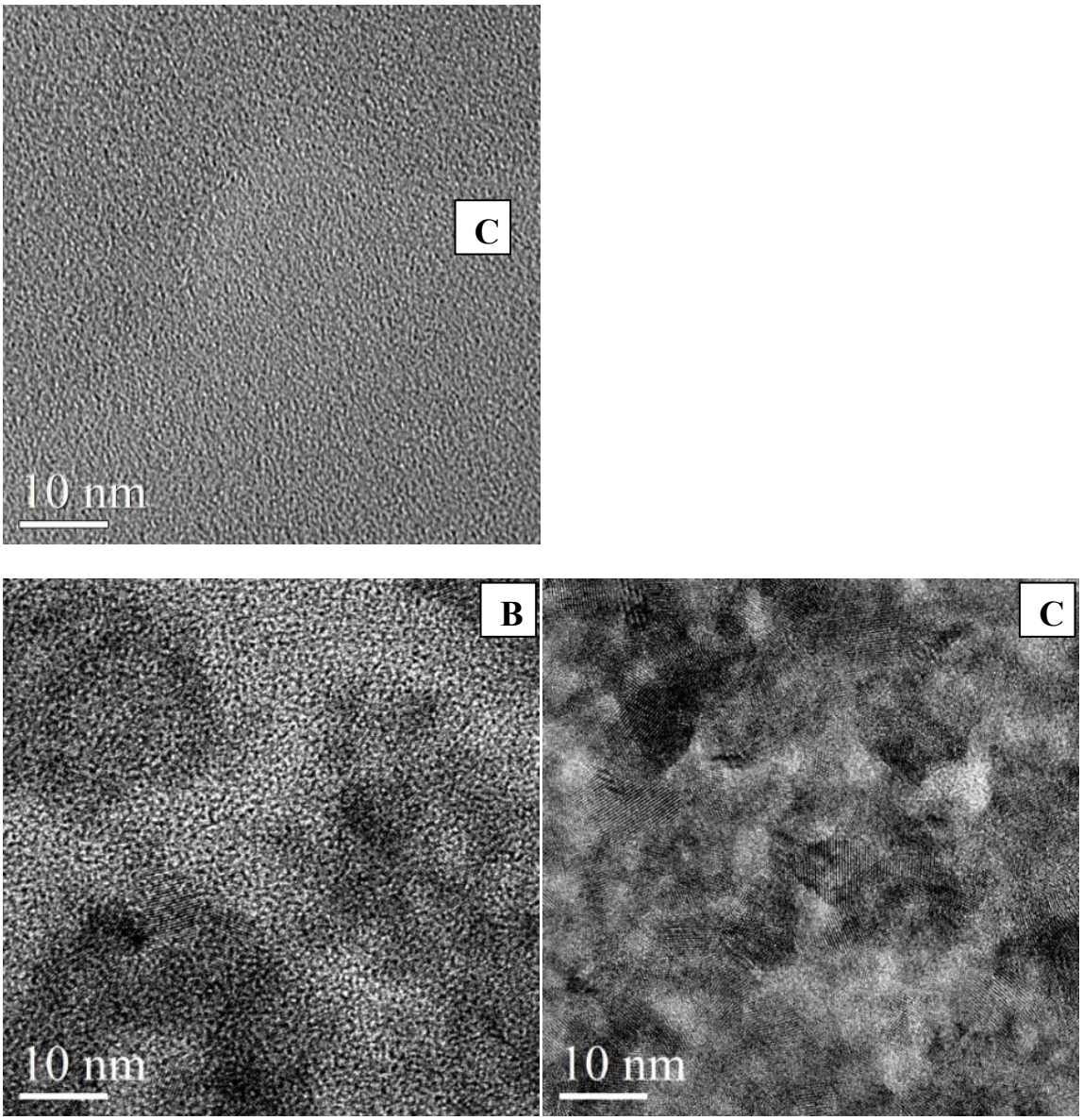

Figure 5. TEM images of photovoltaic thin films with different compositions: Pol (A), CdS(2X) (B), and CdS(2X)/ZnS(2X) (C).

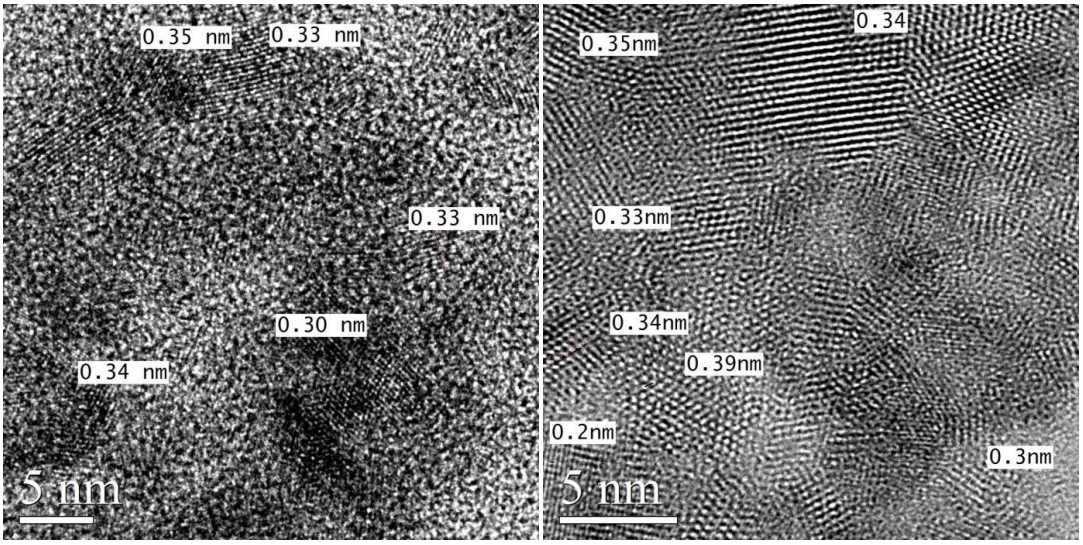

Figure 6. HRTEM images of hybrid thin films with CdS NPs (left) and CdS/ZnS NPs (right).

2.3.2 EDX analysis

Table 1 displays EDX analysis for the elemental composition of thin films with different compositions, and the monitored elements are sulfur, cadmium, and zinc. No zinc was found in the thin film made solely of **Pol** (1) and hybrid material made of **Pol** and CdS (2) and (3), while the films made of **Pol** and CdS/ZnS (4) and (5) were confirmed to have zinc in their composition. All of these samples contain sulfur and cadmium in their composition. This information assures that zinc is successfully introduced to the polymer matrix. In film **(1)**, the cadmium atomic concentration is extremely small compared to sulfur as the only cadmium present are the seed atoms. The thin films (2) and (3) which have gone through two and four CdS growth cycles have S:Cd ratios of 2.8:1 and 2.3:1, respectively. The non-significant difference in elemental

composition between (2) and (3) suggest the uniform incorporation of sulfur and cadmium atoms to the polymer matrix. Core/shell sample (4) and (5) have S:Cd:Zn ratios of 3.1:1.0:1.2 and 5.0:1.0:2.4, respectively. The ratio and the increase in NP size after shell growth suggest that sulfur and zinc uniformly incorporate onto the CdS core to form a ZnS shell.

No.	Sample	S	Cd	Zn
1	**Pol**	327.8	1.0	--
2	**CdS(2X)**	2.8	1.0	**--**
3	**CdS(4X)**	2.3	1.0	**--**
4	**CdS(2X)/ZnS(1X)**	3.7	1.0	1.2
5	**CdS(2X)/ZnS(2X)**	5.0	1.0	2.4

Table 1. Summary of EDX composition for thin film composed of **Pol** and CdS or CdS/ZnS of various compositions grown on **Pol.**

2.3.3 Photo-oxidation analysis

The photo-oxidation process of the thin films was monitored with UV-Vis absorption spectroscopy and X-ray photoelectron spectroscopy (XPS). UV-Vis absorption spectra reveal that the CdS/ZnS NPs were able to delay the photo-oxidation more efficiently than the polymer by itself or the polymer with the CdS NPs only. The thin films absorb visible light in the range of 300 nm - 600 nm and the maximum absorption peak is at 500 nm. It is observed that the longer the films were exposed to air and visible light, the more the

absorption peak at 500 nm decayed. In addition, maximum absorption peak at 500 nm shows a blue-shift after 835 hours of being photo-oxidized (Figure 7). Interestingly, the blue-shift occurs slower in the thin films with core/shell structured NPs than the films made of polymer only or with core only NPs. The maximum absorption peak shifted to 420 nm, 400 nm, and 350 nm in thin films with CdS(2X)/ZnS(4X), CdS(2X) and Pol respectively. The degradation consists of the reduction of film optical absorption and the blue shift of the main absorption band indicating the destruction of some of the thiophene rings and therefore the interruption of the conjugated system; these problems in optical absorption were reported to lower the efficiency of the solar device.[43] It is observed that after 835 exposure hours, the absorption at 500 nm of degraded film made of polymer is only 14.4% in comparison to the freshly prepared one, while the film with CdS(2X) NPs retains 17.2%, film with CdS(2X)/ZnS(1X) NPs retains 21.4%, and film with CdS(2X)/ZnS(4X) NPs retains 47.9% (Figure 8). This is consistent with the hypothesis that the CdS/ZnS core/shell structure can delay the photo-oxidation process of the photovoltaic cells, and the thicker the ZnS shell is, the longer the cell can last.

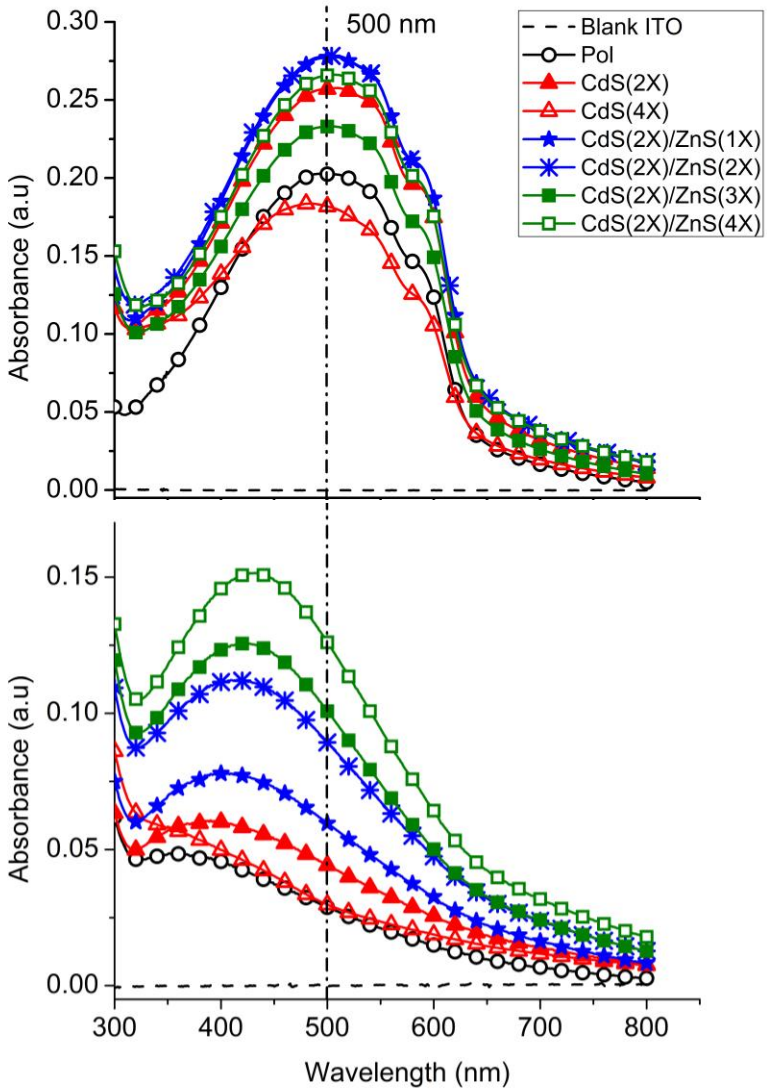

Figure 7. UV-Vis absorption spectra of thin films of various compositions exposed to atmosphere and visible light in 0 hour (top) and 835 hours (bottom).

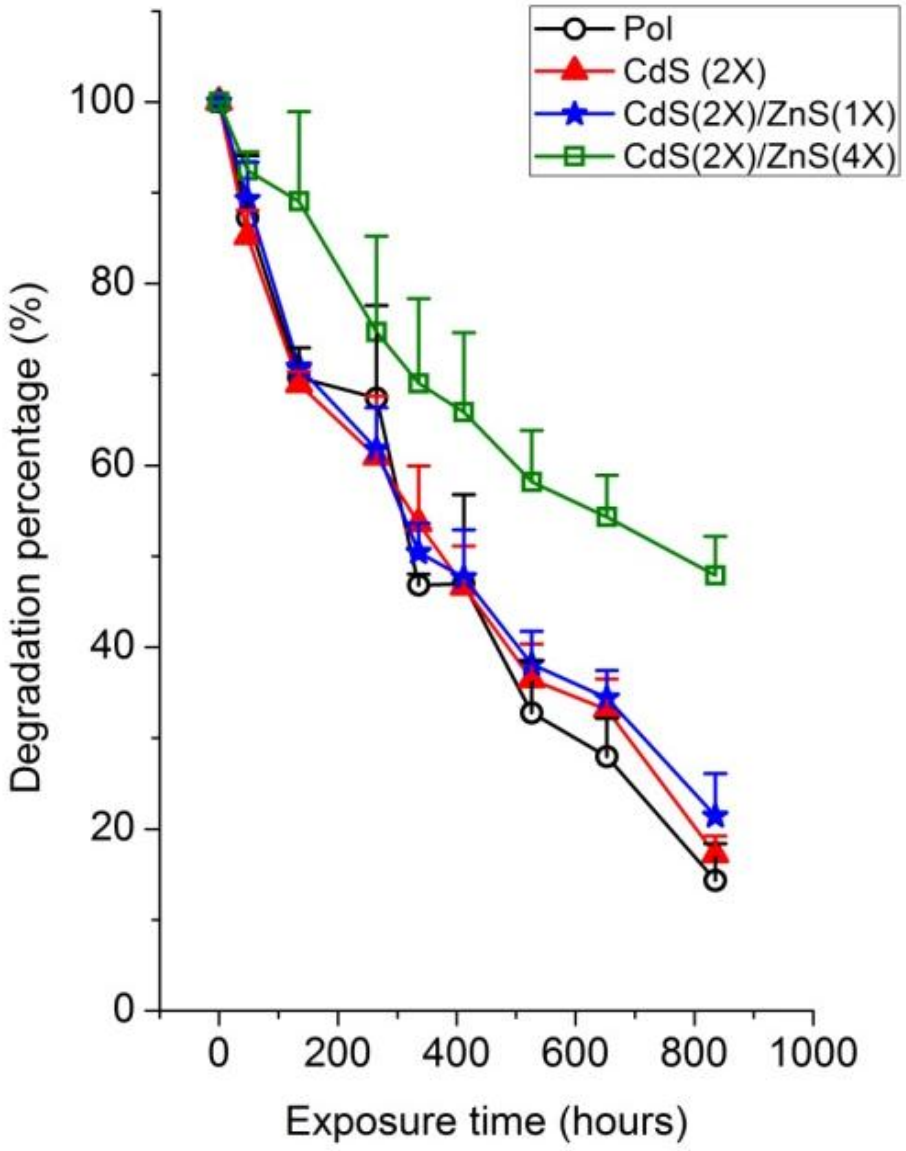

Figure 8. Degradation percentage of the optical absorption at 500 nm of thin films with various compositions

2.3.4 XPS analysis

Figure 9 shows the S 2*p* XPS spectra for thin film composed of **Pol** and CdS(2X), CdS(2X)/ZnS(2X), or CdS(2X)/ZnS(4X) NPs. There are three XPS signals detected for all samples, i.e. peaks at 162 eV, 164 eV, and 165 eV. The intensity of these three peaks decayed as the thin films were photo-oxidized. XPS peaks at 162 eV is assigned to unoxidized S 2*p* originating from Cd-S[49] and Zn-S.[50] The polymer-based sulfur gives rise to the spin-orbit splitting doublet (S $2p_{3/2}$ and S $2p_{1/2}$), which are detected at 164 eV and 165 eV.[51] As the thin films were exposed to air and visible light after 120 hours and 800 hours, a new XPS peak grew in at 168 eV. This peak is indicative of oxidized S 2*p* originating from $ZnSO_4$,[50] sulfonic acid,[52] sulfoxides, and sulfones.[49] It is observed that the XPS peak at 162 eV is significantly more intense in the freshly prepared sample with CdS(2X)/ZnS(4X) NPs when compared to the others, and it was reduced after the first 120 hours of photo-oxidation. This indicates the existence of ZnS shell in the sample, and suggests that ZnS is the species oxidized the most in the first 120 hours of photo-oxidaiton while maintaining good optical absorption of the thin film. In addition, in the sample with CdS(2X) NPs, the XPS peak at 162 eV was gone after 800 hours of photo-oxidation, while it was retained in the sample with the core/shell NPs. This complete reduction of the XPS peak at 162 eV demonstrates that the ZnS shell can protect the CdS NP from being photo-oxidized. Overall, it can be concluded from the XPS data that photo-oxidation involves the oxidation of sulfur originating from both the polymer and the NPs.

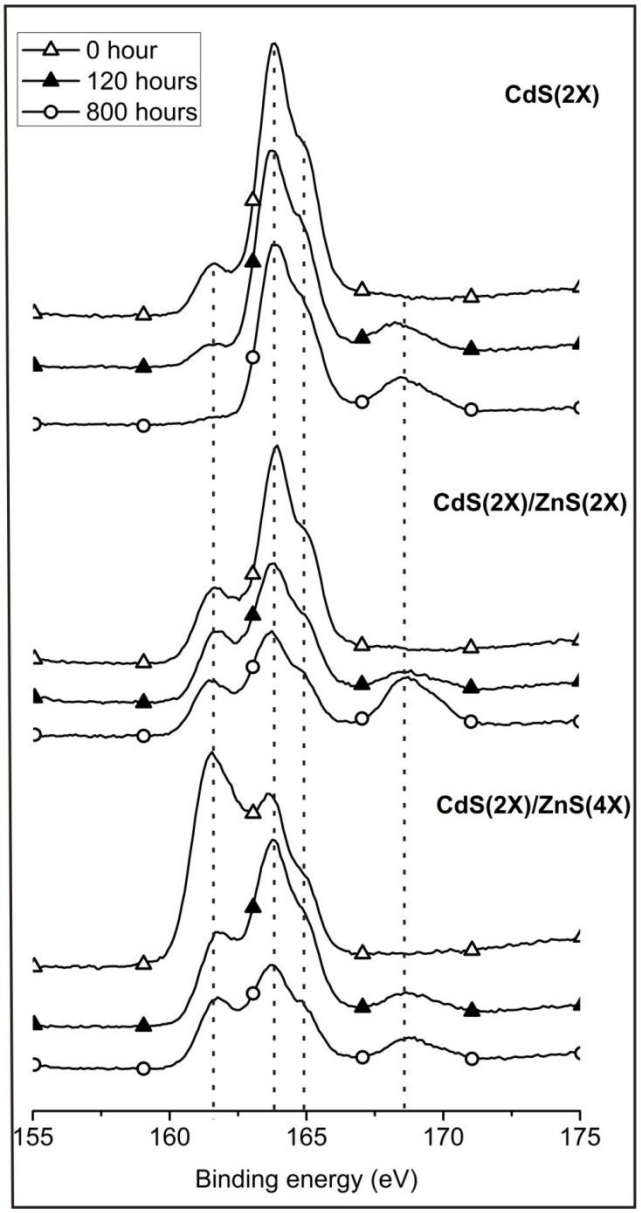

Figure 9. XPS core-level spectra of sulfur S 2*p* at different stages of degradation of thin films composed of **Pol** and CdS(2X) NPs (top), **Pol** and CdS(2X)/ZnS(2X) NPs (middle), and **Pol** and CdS(2X)/ZnS(4X) NPs (bottom).

2.4 Conclusion

It is not completely certain to conclude about the core/shell structure of the NPs grown. Each of the characterization technique brings about more than one possibility of the structure of the NPs. When zinc is chemically introduced to CdS NPs, the possible structures for the newly formed NPs can be core/shell, alloy, or independent CdS NPs and ZnS NPs. UV-Vis and XPS spectra prove that only core/shell structure is possible as alloy structured NPs or independent CdS and ZnS should not bring about hole confinement effects which help to delay photo-oxidation. The fact that the size of the NPs increases after shell growth steps suggest that the NP structure can be core/shell or alloy only. Last, EDX analysis showing the existence of Zn after shell growth could be consistent with either core/shell, alloy, or independent CdS NPs and ZnS NPs.

In conclusion, we have demonstrated the method of growing the core/shell NPs by growing the shell around the CdS core which is embedded in a metallopolymer matrix using the seeded growth method at room temperature. The core/shell effect of delaying photo-oxidation has been confirmed with UV-Vis absorption spectra, and the thin film with CdS/ZnS NPs can help extend the photovoltaic thin film stability up to three times longer than the one with CdS NPs alone. The photo-oxidation mechanism illuminated with the XPS spectra is expected to occur with the destruction of the bithiophene ring structure and therefore the conjugation system. TEM analysis is helpful to characterize the core/shell structure but further investigation is crucial for the confirmation of core/shell structure.

Chapter 3

Direct Synthesis of CIGS Nanoparticles within Conducting Metallopolymer Matrix for Hybrid Photovoltaic

3.1 Introduction

Polycrystalline CIGS is favorable among the investigated thin film photovoltaic absorber materials thanks to its high optical absorption coefficient, tunable band gap and benign grain boundaries.[53] During the last five years, the research trend in developing low cost manufacturing of $CuIn_xGa_{1-x}Se_2$ (CIGS) solar devices are attractive due to the fact that industrial CIGS solar cell production is based on vacuum processes, which demand high investment into production machines. Research towards low cost techniques for CIGS solar device manufacture commonly focus on simple and non-vacuum deposition methods in combination with the control of film composition at the molecular level. A maximum CIGS cell efficiency is 19.3% using three-stage co-evaporation process. Figure 10 summarizes the non-vacuumed methods in direct manufacturing of CIGS thin films. They are electrodeposition, spray pyrolysis and paste coating which all followed by selenization and annealing steps.[54]

The project herein brings in a new and simple approach to fabricate polymer based CIGS thin films, using the seeded growth method described in section 1.3.3. This CIGS thin film is a composite made from CIGS NPs grown within the conducting metallpolymer electropolymerized from solution of copper complex containing polymerizable bithiophene end groups attached to a salen-type ligand. The salen-type ligand is the binding site for the copper [39] ions which is the nucleation site for the CIGS NPs. This method is as promising as it is simple and the low-cost process at room temperature employs electropolymerization and seeded growth methods.

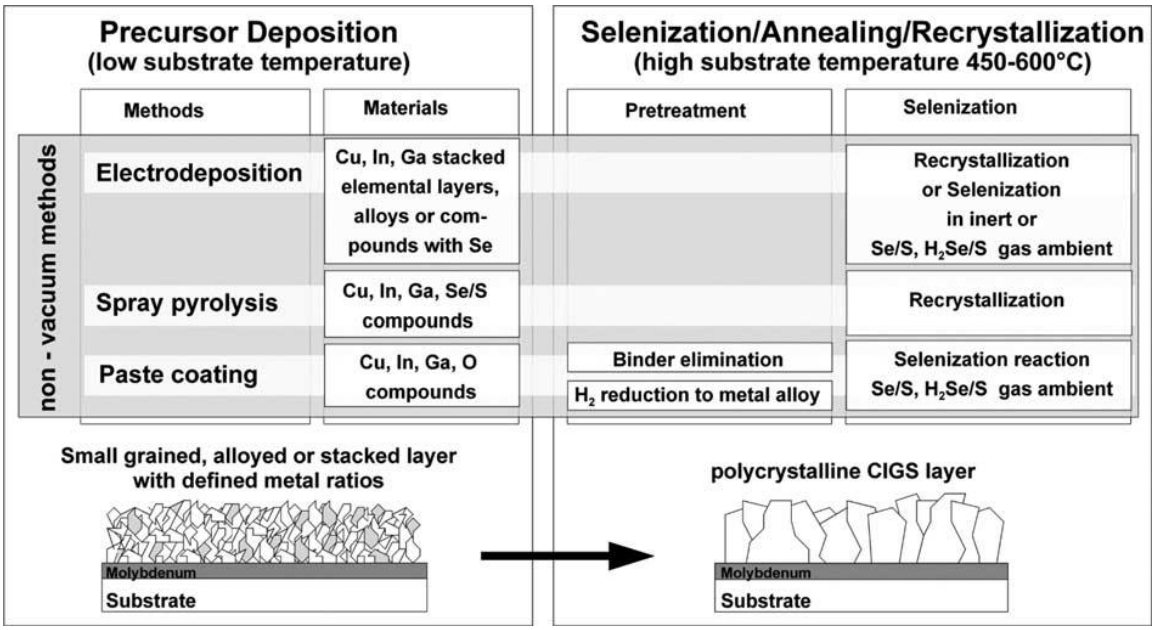

Figure 10. Low cost, non-vacuum methods for CIGS deposition.[54]

3.2 Experimental

The following chemicals were used as received: Copper nitrate trihydrate (Matheson Coleman & Bell), Indium nitrate hydrate (Alfa Aesar), Gallium nitrate hydrate (Alfa Aesar). All solvents were dried using an Innovative Technology, Pure Solv solvent purifier. All reactions were performed with standard Schlenck techniques. Nanoparticle characterization was performed with Transmission Electron Microscope (TEM).

3.2.1 Synthesis of copper salen complex (A)

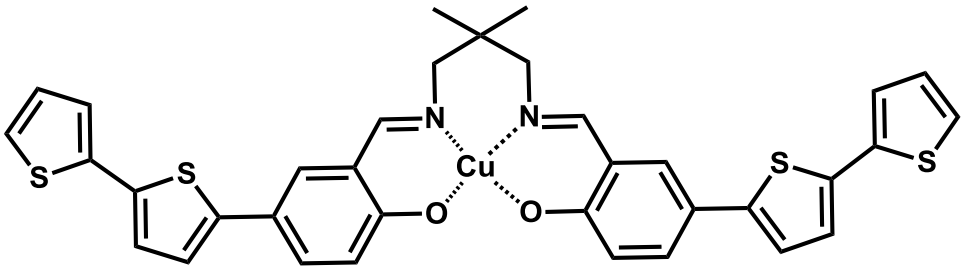

Synthesis of copper salen complex was developed by Mejía from our group.[55]

3.2.2. Electropolymerization

Metallopolymer thin film **Pol** was electropolymerized from a $3x10^{-4}$ M CH_2Cl_2 solution of **(A)** by cycling between -0.5V and 1.5V at ν=100 mVs^{-1} for 2 scans under nitrogen atmosphere in a glovebox using GPES system from Eco. Chemie B. V.. The electrolyte used was 0.1 M tetrabutylammonium hexaflourophosphate [(*n*-Bu)$_4$N][PF_6]

TABPF6. Electrochemical experiments were performed in a three-electrode cell with a $Ag/AgNO_3$ non-aqueous reference electrode, a working electrode, and a Pt wire coil counter electrode.[55] Working electrode is onto a carbon coated gold TEM grids purchased from Electron Microscopy Sciences.

3.2.3 Seeded Growth Procedure for CIGS Nanoparticles

The growth of CIGS NPs was achieved by sequentially treating the films with $3x10^{-4}$ M cation solution containing Cu^{2+}, In^{3+}, and Ga^{3+} (CIG^{+}) and $3x10^{-4}$ M anion solution containing Se^{2-}. CIG^{+} solution is made of $Cu(NO_3)_2 \cdot 3H_2O$, $In(NO_3)_3 \cdot xH_2O$, and $Ga(NO_3)_3 \cdot xH_2O$ in dry Acetonitrile (ACN) and methanol. Se^{2-} solution is prepared according to literature.[56] A CIGS growth cycle consists of the three following steps. The electropolymerized thin films were soaked in CIG^{+} in dry ACN/methanol ($4x10^{-4}$ M) for one minute, and then rinsed thoroughly with dry ACN. The films were then soaked in a solution of Se^{-} in dry ACN ($4x10^{-4}$ M) for one minute followed by rinsing with dry ACN. Last, the films then rinsed soaked in the same CIG^{+} solution for one minute and rinsed thoroughly with dry ACN. The thin film which went through 1 cycle (1X) of CIGS growth is named CIGS(1X).

3.2.4 Transmission Electron Microscope

TEM experiments were performed using JEOL 2010F microscope configured with Oxford INCA energy dispersive spectrometer. NP analysis was done using Gatan Digital Micrograph software. A sample for TEM characterization were prepared by

electropolymerizing a thin film of **Pol** onto a carbon coated gold TEM grids purchased from Electron Microscopy Sciences. The films were kept in air free environment and NPs were grown with the seeded growth method described above.

3.3 Results and discussion

3.3.1 TEM images and analysis of NPs size and d-spacing

According NPs size analysis based on TEM images (Figure 11), the CIGS (2X) NPs' average size is 2.7 nm x 2.4 nm while CIGS (4X) NPs's average size is 3.8 nm x 3.0 nm. It is observed that after two growth cycles, the NPs expand their size in the elongation fashion. Experimentally measured d-spacing for CIGS (4X) NPs is 0.33 nm which corresponds to the (220) orientation of the $CuIn_{0.7}Ga_{0.3}Se_2$ nanocrystals.[57] It is observed that CIGS NPs remain amorphous after two growth cycles (Figure 11B) and the crystallized after two more growth cycles (Figure 11C). Accordingly, the more growth cycles the films go through, the bigger and more crystallized the CIGS NPs will be.

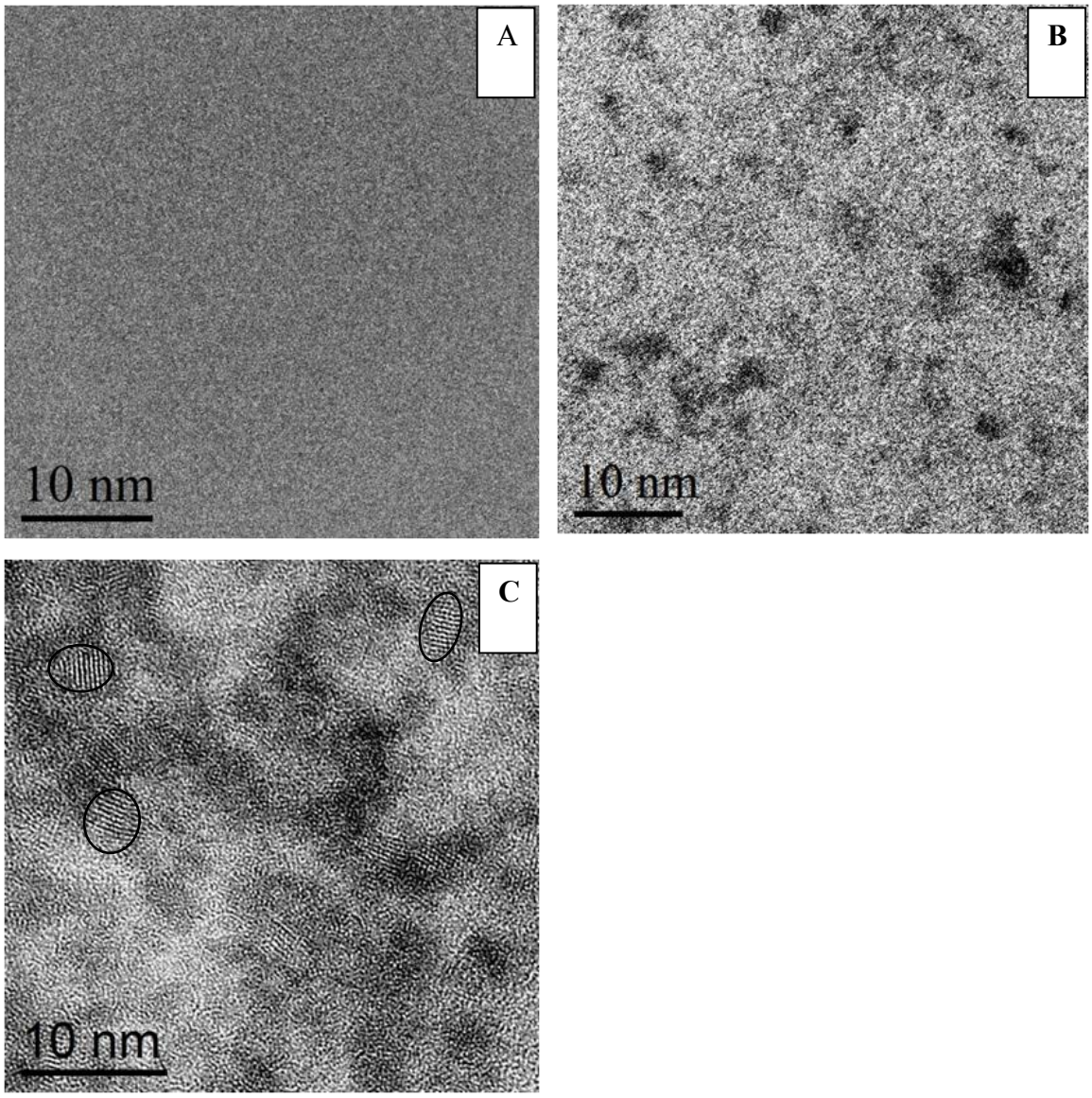

Figure 11. TEM images of thin film made of different compositions: Pol (A), Pol and CIGS (2X) (B), and Pol and CIGS (4X) (C).

3.3.2 EDS analysis

EDX analysis for the CIGS NPs' composition is reported in the Table 2. Copper concentration is always the highest in the two types of NPs, which is 53.6% for CIGS(2X) NPs and 46.7% for CIGS(4X) NPs. Gallium concentration in CIGS(2X) NPs, which is 11.9%, is slightly higher than CIGS(4X) NPs which is 7.4%. On the other hand, selenium concentration in CIGS(2X) NPs which is 22.3%, is lower than CIGS(4X) NPs, which is 33.5%. The Indium concentration in CIGS(2X) NPs and CIGS(4X) NPs compositions are both approximately 12%. EDX spectra of the thin films made of **Pol**, and thin films made of **Pol** and CIGS(2X) or CIGS(4X) NPs are provided respectively in the Figure 12, 13 and 14. It is observed that the Ga, Se, and In peaks are only detected in EDX spectra of the thin films made of CIGS(2X) and CIGS(4X) NPs. Overall, the EDX results suggest that the coordination of copper ions and gallium ions to the forming CIGS NPs is slower than Se and In ions.

	CIGS (2X)		**CIGS (4X)**	
	Average (%)	**Std. Dev. (%)**	**Average (%)**	**Std. Dev (%)**
Cu	53.6	*1.5*	46.7	*6.4*
Ga	11.9	*1.3*	7.4	*1.4*
Se	22.3	*2.5*	33.5	*8.9*
In	12.3	*2.7*	12.4	*2.9*

Table 2. Summary of EDX composition for thin film composed of CIGS(2X) or CIGS(4X) NPs grown on **Pol.**

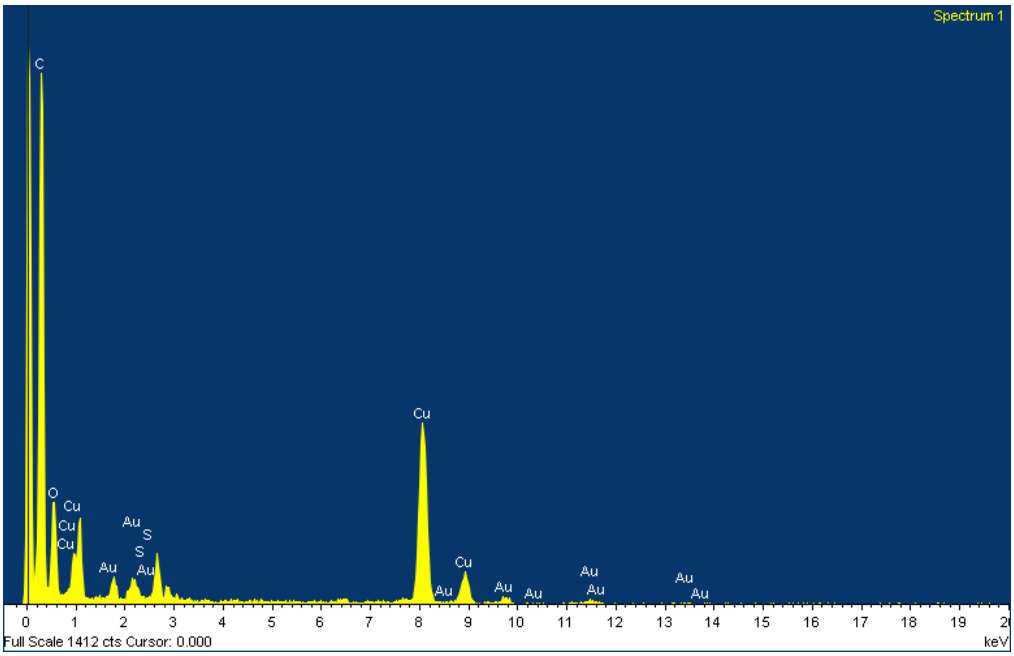

Figure 12. EDX spectra of thin film made of **Pol**.

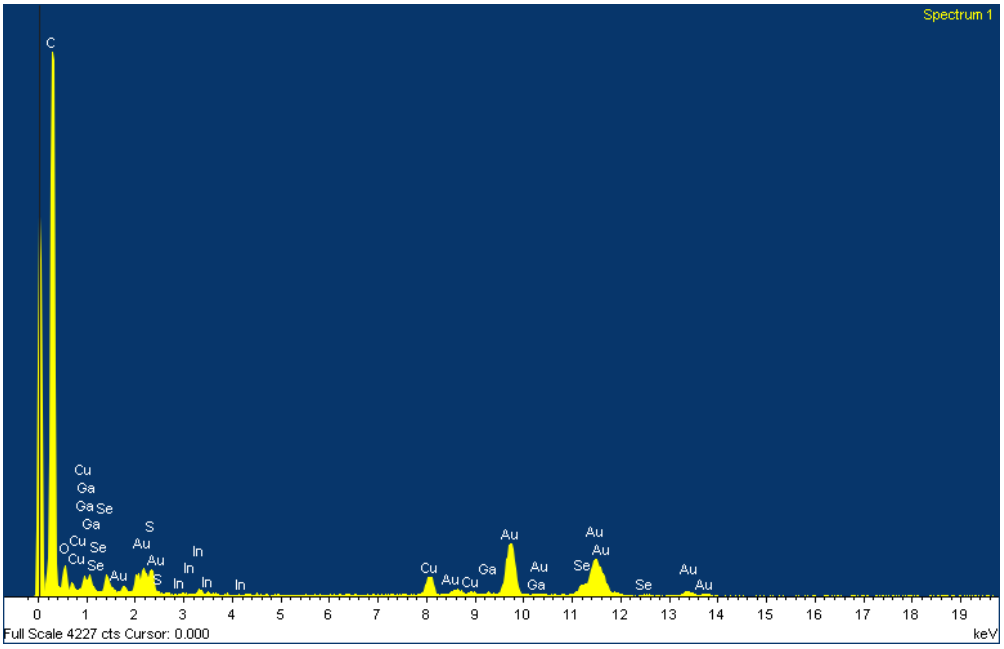

Figure 13. EDX spectra of thin film composed of **Pol** and CIGS (2X) NPs.

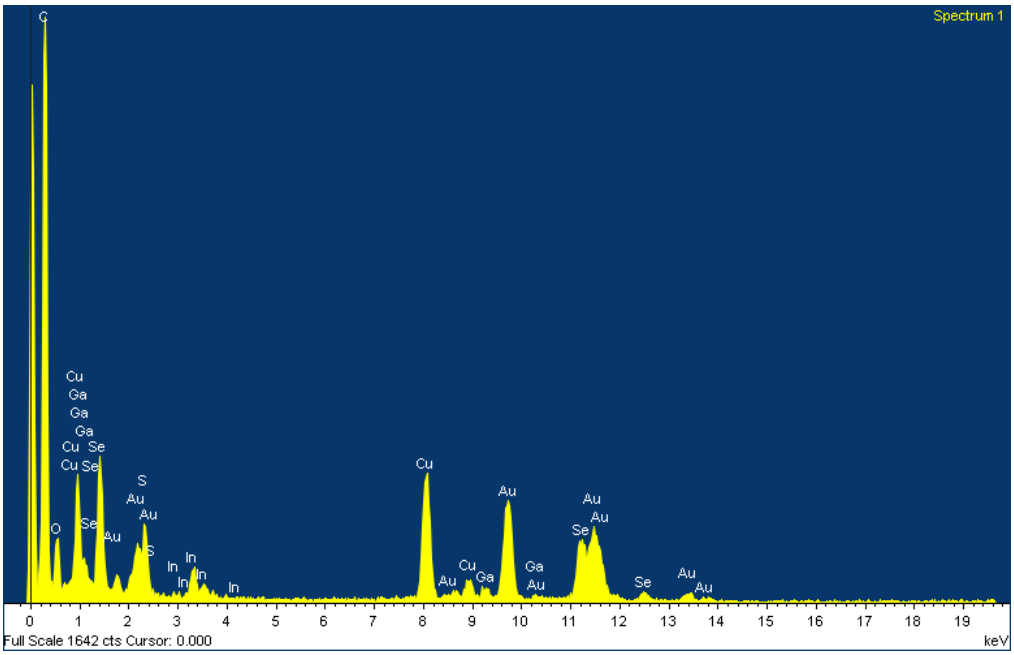

Figure 14. EDX spectra of thin film composed of **Pol** and CIGS (4X) NPs.

3.4 Conclusions

In conclusion, the polymer based CIGS thin films have been successfully fabricated using electropolymerization to form conducting metallopolymer and the seeded growth method to form crystallized CIGS NPs. Future work will focus on tuning the CIGS composition by adjusting the concentration of the metal cation and selenium anion precursor, and this is considered for further investigation.

REFERENCES

(1) Friend, R. H. *Pure Appl. Chem.* **2001**, *73*, 425.

(2) Wang, G.; Swenson, J.; Moses, D.; Heeger, A. J. *J. Appl. Phys.* **2003**, *93*, 6137.

(3) Hebner, T. R.; Wu, C. C.; Marcy, D.; Lu, M. H.; Sturm, J. *Appl. Phys. Lett.* **1998**, *72*, 519.

(4) Chang, S.; Liu, J.; Bharathan, J.; Yang, Y.; Onohara, J.; Kido, J. *Adv. Mater.* **1999**, *11*, 734.

(5) Pschenitzha, F.; Sturm, J. C. *Appl. Phys. Lett.* **1999**, *74*, 1913.

(6) Rogers, J. A.; Bao, Z.; Raju, V. R. *Appl. Phys. Lett.* **1998**, *72*, 2716.

(7) Shaheen, S. E.; Radspinner, R.; Peyghambarian, N.; Jabbour, G. E. *Appl. Phys. Lett.* **2001**, 2996.

(8) Coakley, K. M.; McGehee, M. D. *Chem. Mater.* **2004**, *16*, 4533.

(9) Saunders, B. R.; Turner, M. L. *Adv. Colloid Interface Sci.* **2008**, *138*, 1-23.

(10) Spanggaard, H.; Krebs, F. C. *Solar Energy Materials and Solar Cells* **2004**, *83*, 125-146.

(11) Hegedus, S.; Luque, A. *Handbook of photovoltaic science and engineering*; John Wiley and Sons: Chichester, 2003.

(12) Gregg, B. A. *J. Phys. Chem. B* **2003**, *107*, 4688.

(13) Bao, Z.; Dodabalapur, A.; Lovinger, A. *Appl. Phys. Lett.* **1996**, *69*, 4108.

(14) Bozano, L.; Carter, S. A.; Scott, J. C.; Malliaras, G. G.; Brock, P. J. *Appl. Phys. Lett.* **1999**, *74*, 1132.

(15) Kline, R. J.; Mcgehee, M. D.; Kadnikova, E. N.; Liu, J.; Frechet, J. M. J. *Adv. Mater.* **2003**, *15*, 1519.

(16) Sirringhaus, H.; Tessler, N.; Friend, R. *Science* **1998**, *280*, 1741.

(17) Babel, A.; Jenekhe, S. *Adv. Mater.* **2002**, *14*, 371.

(18) Sze, S. M. *VLSI Technology*; 2nd ed.; McGraw-Hill Publishing Co.: New York, 1988.

(19) Halls, J. J. M.; Pichler, K.; Friend, R. H.; Moratti, S. C.; Holmes, A. B. *Appl. Phys. Lett.* **1996**, *68*, 3120-3122.

(20) Leif, A. A. P.; Lucimara, S. R.; Olle, I. *J. Appl. Phys.* **1999**, *86*, 487-496.

(21) Theander, M.; Yartsev, A.; Zigmantas, D.; Sundstroum, V.; Mammo, W.; Andersson, M. R.; Inganas, O. *Phys. Rev. B* **2000**, *61*, 12957.

(22) Savenije, T. J.; Warman, J. M.; Goossens, A. *Chem. Phys. Lett.* **1998**, *287*, 148.

(23) Haugeneder, A.; Neges, M.; Kallinger, C.; Spirkl, W.; Lemmer, U.; Feldmann, J.; Scherf, U.; Harth, E.; Gügel, A.; Müllen, K. *Phys. Rev. B* **1999**, *59*, 15346.

(24) Ginger, D. S.; Greenham, N. C. *Phys. Rev. B* **1999**, *59*, 10622.

(25) Greenham, N. C.; Peng, X.; Alivisatos, A. P. *Phys. Rev. B* **1996**, *54*, 17628.

(26) Baoquan, S.; Henry, J. S.; Anoop, S. D.; Sebastian, W.; Neil, C. G. *J. Appl. Phys.* **2005**, *97*, 014914.

(27) Huynh, W. U.; Dittmer, J. J.; Alivisatos, A. P. *Science* **2002**, *295*, 2425-2427.

(28) Gur, I.; Fromer, N. A.; Chen, C.-P.; Kanaras, A. G.; Alivisatos, A. P. *Nano Lett.* **2006**, *7*, 409-414.

(29) Liu, C. Y.; Holman, Z. C.; Kortshagen, U. R. *Nano Lett.* **2009**, *9*, 449-452.

(30) de Freitas, J. N.; Grova, I. R.; Akcelrud, L. C.; Arici, E.; Sariciftci, N. S.; Nogueira, A. F. *J. Mater. Chem.* **2010**, *20*, 4845.

(31) Liu, J.; Tanaka, T.; Sivula, K.; Alivisatos, A. P.; Frechet, J. M. J. *J. Amer. Chem. Soc.* **2004**, *126*, 6550-6551.

(32) Yang, S.; Yan, D.; Shi, A. C. *Macromolecules* **2006**, *39*, 4168-4174.

(33) Nguyen, L. H.; Hoppe, H.; Erb, T.; Günes, S.; Gobsch, G.; Sariciftci, N. S. *Adv. Funct. Mater.* **2007**, *17*, 1071-1078.

(34) Sun, B.; Marx, E.; Greenham, N. C. *Nano Lett.* **2003**, *3*, 961-963.

(35) Napper, D. H. *Polymeric stabilization of colloidal dispersions*; Academic Press: London, 1983.

(36) Ghezelbash, A.; Koo, B.; Korgel, B. A. *Nano Lett.* **2006**, *6*, 1832-1836.

(37) Dayal, S.; Kopidakis, N.; Olson, D. C.; Ginley, D. S.; Rumbles, G. *J. Am. Chem. Soc.* **2009**, *131*, 17726-17727.

(38) Di Luccio, T.; Laera, A. M.; Tapfer, L.; Kempter, S.; Kraus, R.; Nickel, B. *J. Phys. Chem. B* **2006**, *110*, 12603-12609.

(39) Radchenko, M.; Lashkarev, G.; Sichkovskyi, V.; Arshakuni, A.; Gubin, S.; Yuhymchuk, V.; Domukhovski, V.; Story, T.; Piryatinskii, Y.; Yurkov, G. *Inorg. Mater.* **2009**, *45*, 468-473.

(40) Mejía, M. L.; Agapiou, K.; Yang, X.; Holliday, B. J. *J. Am. Chem. Soc.* **2009**, *131*, 18196-18197.

(41) Holliday, B. J.; Swager, T. M. *Chem. Commun.* **2005**, 23-36.

(42) Jørgensen, M.; Norrman, K.; Krebs, F. C. *Sol. Energy Mater. Sol. Cells* **2008**, *92*, 686-714.

(43) Hintz, H.; Egelhaaf, H. J.; Peisert, H.; Chassé, T. *Polym. Degrad. Stab.*, *95*, 818-825.

(44) Spanhel, L.; Haase, M.; Weller, H.; Henglein, A. *J. Am. Chem. Soc.* **1987**, *109*, 5649.

(45) Peng, X.; Schlamp, M. C.; Kadavanich, A. V.; Alivisato, A. P. *J. Am. Chem. Soc.* **1997**, *119*, 7019.

(46) Torimoto, T.; Reyes, J. P.; Iwasaki, K.; Pal, B.; Shibayama, T.; Sugawara, K.; Takahashi, H.; Ohtani, B. *J. Am. Chem. Soc.* **2002**, *125*, 316.

(47) Quan, Z.; Wang, Z.; Yang, P.; Lin, J.; Fang, J. *Inorg. Chem.* **2007**, *46*, 1354.

(48) Kim, M. R.; Kang, Y.; Jang, D. *J. Phys. Chem. C* **2007**, *111*, 18507.
(49) Sato, K.; Kojima, S.; Hattori, S.; Chiba, T.; Ueda-Sarson, K.; Torimoto, T.; Tachibana, Y.; Kuwabata, S. *Nanotechnology* **2007**, *18*, 465702.
(50) Lu, S. W.; Schmidt, H. K. *Mater. Res. Bull.* **2008**, *43*, 583.
(51) Kang , E. T.; G., N. K. *Phys. Rev. B* **1991**, *44*, 10461.
(52) Coen, M.; Keller, B.; Groening, P.; Schlapbach, L. *J. Appl. Phys.* **2002**, *92*, 5077.
(53) Schock, H. W.; Noufi, R. *Prog. Photovoltaics* **2000**, *8*, 151.
(54) Kaelin, M.; Rudmann, D.; Tiwari, A. N. *Sol. Energy* **2004**, *77*, 749.
(55) Mejía, M. L. dissertation, The University of Texas at Austin, 2010.
(56) Lee, H.; Wang, M.; Chen, P.; Gamelin, D. R.; Zakeeruddin, S. M.; Grätzel, M.; Nazeeruddin, M. K. *Nano Lett.* **2009**, *9*, 4221.
(57) Hsu, W. H.; Hsiang, H. I.; Chang, Y. L.; Ray, D. T.; Yen, F. S. *J. Am. Ceram. Soc.*, published online Apr 1, 2011 (doi: 10.1111/j.1551-2916.2011.04488.x).